

# Resolving the compact H II regions in N160A with *HST* \*

M. Heydari-Malayeri<sup>1</sup>, V. Charmandaris<sup>2</sup>, L. Deharveng<sup>3</sup>, F. Meynadier<sup>1</sup>, M.R. Rosa<sup>4, \*\*</sup>, D. Schaerer<sup>5</sup>,  
and H. Zinnecker<sup>6</sup>

<sup>1</sup> DEMIRM, Observatoire de Paris, 61 Avenue de l'Observatoire, F-75014 Paris, France

<sup>2</sup> Cornell University, Astronomy Department, 106 Space Sciences Bldg., Ithaca, NY 14853, USA

<sup>3</sup> Observatoire de Marseille, 2 Place Le Verrier, F-13248 Marseille Cedex 4, France

<sup>4</sup> Space Telescope European Coordinating Facility, European Southern Observatory, Karl-Schwarzschild-Strasse-2, D-85748 Garching bei München, Germany

<sup>5</sup> Observatoire Midi-Pyrénées, 14, Avenue E. Belin, F-31400 Toulouse, France

<sup>6</sup> Astrophysikalisches Institut Potsdam, An der Sternwarte 16, D-14482 Potsdam, Germany

Received 24 September 2001 / Accepted 29 October 2001

**Abstract.** Using high-resolution imaging with the *Hubble Space Telescope*, we study the Large Magellanic Cloud H II region N160A and uncover several striking features of this complex massive star-forming site. The two compact high excitation H II blobs (HEBs) A1 and A2 are for the first time resolved and their stellar content and morphology is revealed. A1, being of higher excitation, is powered by a single massive star whose strong wind has created a surrounding bubble. A2 harbors several exciting stars enshrouded inside large quantities of dust. The whole N160A nebula is energized by three star clusters for which we obtain photometry and study their color-magnitude diagram. The H II region is particularly dusty, with extinction values reaching an  $A_V \sim 2.5$  mag in the visible, and it is separated from the molecular cloud by an outstanding ionization front. A previously detected infrared young stellar object is also accurately located with respect to the H II region.

**Key words.** Stars: early-type – dust, extinction – H II regions – individual objects: N160A – Galaxies: Magellanic Clouds

## 1. Introduction

The region of 30 Doradus has long been identified as a unique star formation site not only in the Large Magellanic Cloud (LMC) but also in our whole Local Group of galaxies. As a result, the regions lying at its periphery have also attracted special attention over the years. In particular, the chain of bright H II regions lying south of 30 Doradus, i.e. N158, N159, and N160 (Henize 1956), not only show several signs of ongoing star formation, such as stars still embedded in their birth cocoons, infrared sources, and masers, but they are also associated with the most important concentration of molecular gas in the LMC (Johannson et al. 1998 and references therein).

This paper is devoted to N160A (NGC 2080), the brightest component of the N160 complex, also known as DEM 284 (Davis et al. 1976) or MC 76 (McGee & Milton 1966), which lies some 30' (450 pc) south of 30 Dor. N160A is a particularly interesting region of star formation as it harbors several compact IR sources (Epchtein et al. 1984, Jones et al. 1986) and OH and H<sub>2</sub>O masers (Caswell & Haynes 1981, Gardener & Whiteoak 1985; Caswell 1995, Whiteoak et al. 1983, Whiteoak & Gardener 1986, Brooks & Whiteoak 1997). It also contains the OB association LH 103 which embodies 41 blue stars (Lucke & Hodge 1970, Lucke 1974).

The first detailed study of N160A was carried out by Heydari-Malayeri & Testor (1986, hereafter Paper I) using extensive optical imaging and spectroscopy of both its gaseous and stellar content, as well as high resolution radio continuum mapping at 843 MHz. They discovered two compact H II regions embedded in the bright H II region N160A. Identified as N160A1 and N160A2, these objects belong to the special class of so-called High Excitation Blobs (HEBs) in the Magellanic Clouds. In contrast to the typical H II regions of the Magellanic

Send offprint requests to: M. Heydari-Malayeri, heydari@obspm.fr

\* Based on observations with the NASA/ESA Hubble Space Telescope obtained at the Space Telescope Science Institute, which is operated by the Association of Universities for Research in Astronomy, Inc., under NASA contract NAS 5-26555. These observations are associated with proposal #8247.

\*\* Affiliated to the Astrophysics Division, Space Science Department of the European Space Agency.

Clouds, which are extended structures spanning several minutes of arc on the sky and powered by a large number of hot stars, HEBs are very dense small regions usually  $5''$  to  $10''$  in diameter. At the distance of the Magellanic Clouds this corresponds to sizes of more than 50 pc for normal H II regions and 1 to 3 pc for the blobs. HEBs are in fact associated with young massive stars just leaving their parent molecular cloud (see Heydari-Malayeri et al. 2001 for references). Using extensive near-IR observations, Jones et al. (1986) studied N160A, obtained the first  $J$  and  $K$  band images of this region, and confirmed the high extinction of both blobs A1 and A2, which they called objects #5 and #9 respectively. More recently, Henning et al. (1998) using near- and mid-IR images and ISO-SWS spectra established the position of the young stellar object in N160A discovered by Epchtein et al. (1984).

In this paper we use observations obtained with the *Hubble Space Telescope* to study the H II region N160A. The higher resolution of *HST* is essential in order to reveal the various emission and dust features of the nebula on the whole and to study the so far elusive HEBs A1 and A2. It is also necessary for better understanding of massive star formation in this interesting region, i.e. to unveil its stellar content and identify the exciting stars, which up to now have remained unknown.

## 2. Observations and data reduction

The observations of N160A were performed with the Wide Field Planetary Camera 2 (WFPC2) on board of the *HST* using several broad- and narrow-band filters. The images taken with the broad-band filters (F300W, F467M, F410M, and F547M) were obtained on February 5, 2000 and aimed at revealing the details of the stellar content of N160A which was centered on the Planetary Camera (PC). The narrow-band filter images (F487N, F503N and F656N) were obtained on May 28, 2000. In that case the target was centered on the WF2 which has larger pixels and lower noise than the PC CCD and is better suited for detecting faint nebular emission. Exposures were taken at different pointings dithered by  $0''.8$  to better sample the point spread function, while the exposure times ranged from 10 to 300 sec (see Table 1 for details).

The data were processed through the standard *HST* pipeline calibration. Multiple images were co-added using the STSDAS task *imcombine*, while cosmic rays were detected and removed with the STSDAS task *crrej*. Normalized images were then created using the total exposure times for each filter. To extract the positions of the stars, the routine *daofind* was applied to the images by setting the detection threshold to  $5\sigma$  above the local background level. The photometry was performed setting a circular aperture of 3–4 pixels in radius in the *daophot*

**Table 1.** Observations of N160A (*HST* GO-8247)

<i>HST</i> filter	Wavelength $\lambda(\text{\AA})$	Exposure time (sec)
F300W (wide-U)	2911	$8 \times 14 = 112$
F410M (Strömgren $v$ )	4090	$8 \times 50 = 400$
F467M (Strömgren $b$ )	4669	$8 \times 35 = 240$
F547M (Strömgren $y$ )	5479	$8 \times 10 = 80$
F487N (H $\beta$ )	4866	$4 \times 260 = 1040$
F502N ([O III])	5013	$4 \times 300 = 1200$
F656N (H $\alpha$ )	6563	$4 \times 260 = 1040$

package in STSDAS.

A crucial point in our data reduction was the sky subtraction. For most isolated stars the sky level was estimated and subtracted automatically using an annulus of 6–8 pixel width around each star. However this could not be done for several stars located in the central region of N160A due to their crowding. In those cases we carefully examined the PSF size of each individual star (FWHM  $\sim 2$  pixels, corresponding to  $0''.09$  on the sky) and did an appropriate sky subtraction using the mean of several nearby off-star positions. To convert into a magnitude scale we used zero points in the Vegamag system, that is the system where Vega is set to zero mag in Cousin broad-band filters. The magnitudes measured were corrected for geometrical distortion, finite aperture size (Holtzman et al. 1995), and charge transfer efficiency as recommended by the *HST* Data Handbook. Our broad-band images reveal 110 stars within the area covered by the PC. Most of them are also visible in the true-color image (Fig. 1), and can be identified using the finder charts presented in Figures 2 and 3. In Table 2 we summarize the photometry for those stars around in the PC2 field of view which are brighter than 19th magnitude in the Strömgren  $y$  filter, as we cannot provide accurate colors for the fainter ones. The photometric errors estimated by *daophot* are smaller than 0.01 mag for the brighter (14–15 mag) stars, while they increase to  $\sim 0.2$  mag for 19 mag stars.

We note that the filter F547M is wider than the standard Strömgren  $y$  filter. To evaluate the presence of any systematic effects in our photometry and color magnitude diagrams due to this difference in the filters, we used the STSDAS package *synphot*. Using synthetic spectra of hot stars, with spectral types similar to those found in H II regions, we estimated the difference due to the *HST* band-passes to be less than 0.002 mag, which is well within the photometric errors.

## 3. Results

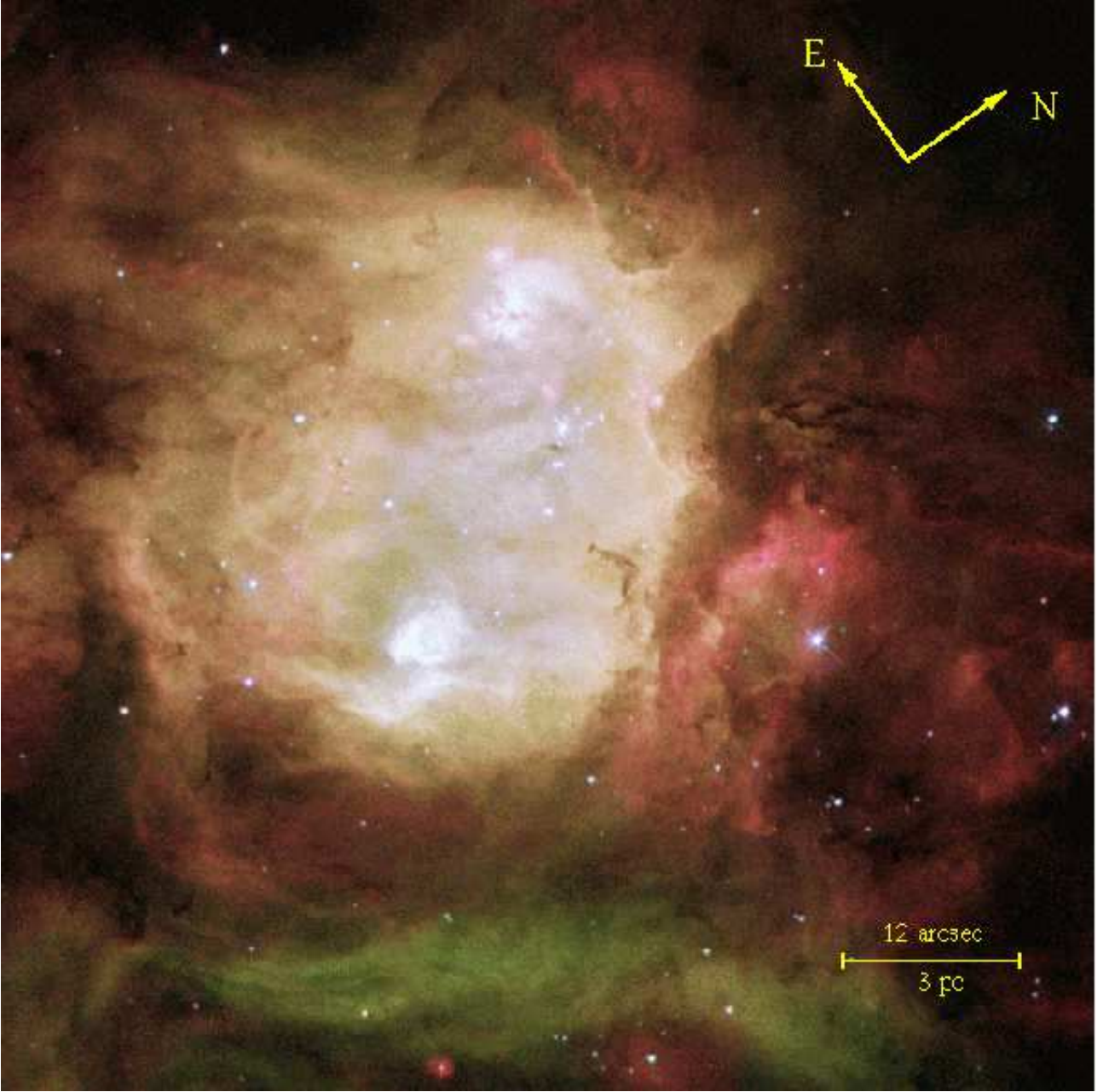


**Fig. 1.** A “true color” composite image of the LMC H II region N160A as seen by *HST*/WFPC2, based on images taken with filters  $H\alpha$  (red),  $[O III]$  (green), and  $H\beta$  (blue). The two bright emission nebulae are the high excitation H II blobs A1 (bottom), and A2 (top). Note the cavity of a mere  $2''.3$  across ( $\sim 0.6$  pc) and the surrounding shell carved by a massive star inside A1 (#22), as well as the bright neighboring ridge. A2 is resolved into a mottled structure due to high dust content and harbors several faint stars. A prominent ionization front borders a high absorption zone to the west where the extinction approaches values higher than  $A_V = 2.5$  mag in the visible. There are also several conspicuous arcs and filaments created by the winds and shocks of the embedded stars as well as a few “tiny” dust pillars, along with a blue star cluster towards the middle of N160A. The whole nebula resembles the features of the head from a “ghost” or “beast” with the HEBs as its eyes and the absorption zone as its mouth! The field size is  $\sim 63'' \times 63''$  ( $\sim 16$  pc  $\times$  16 pc).

### 3.1. Morphology

Ground-based images show N160A as a very bright and rather elongated emission nebula of size  $\sim 35'' \times 25''$ , corresponding to  $8.8 \times 6.3$  pc (Paper I). Three bright

stars were identified within the nebula along with the two outstanding bright compact H II “blobs” A1 and A2 separated by  $\sim 20''$  (5 pc). However, those images were incapable of resolving the structure of the blobs and the

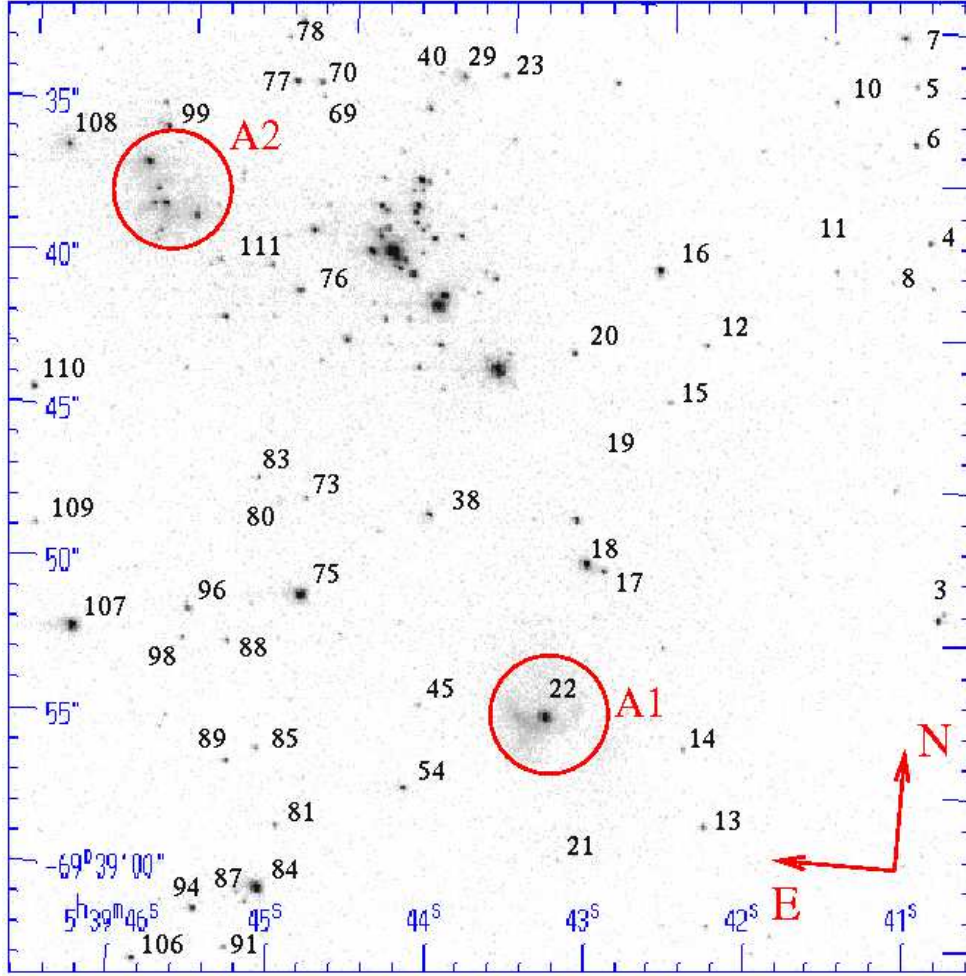


**Fig. 2.** An *HST*/WFPC2 image of LMC N160A taken with the Strömgren  $y$  filter (F547M) showing the stellar content of the giant H II region. Star #22 is associated with A1, while stars #108, #29, and #72 are identified with the three distinct red sources in the upper center area of Fig. 1. The locations of A1 and A2 are marked and the unlabeled stars are identified in the two subsamples displayed in Fig. 3 and the photometry is presented in Table 2. The field size is  $\sim 32'' \times 32''$  ( $\sim 8 \text{ pc} \times 8 \text{ pc}$ ), and orientation is indicated.

star cluster associated with those three bright members seen as stars #24, #35, and #58 plus their adjacent components in Fig. 2 presented below.

A true color image of N160A, obtained with WFPC2 (Fig. 1), displays a magnificent scene with evidence of high activity from newborn massive stars: outstanding emission ridges sculpted by powerful shocks and winds, arcs and filaments, several “small” dust pillars protruding from hot gas, prominent dust concentrations confining the ionized gas at the western side where a long undulating ionization front is visible, etc. More importantly, the *HST* images for the first time resolve the HEBs revealing their morphologies and stellar contents. The compact H II region A1, which is the brightest part of the whole N160A nebula, shows a “tiny” cavity or bubble, some  $2''.3$  across, carved by the strong wind of a relatively bright star (#22). The cavity has a remarkably thin edge of  $< 0''.2$ , but becomes thicker and more luminous

in its southeastern part. The central star appears to be offset towards that direction. A1 is separated by a low brightness gap from the long wavy-form bright ridge seen at  $\sim 3''$  from star #22. The other HEB, A2, is  $3''$  in diameter and displays a rather different structure. It has a patchy appearance marked by the presence of several thin absorption lanes, the main one situated towards its central parts, and unlike A1, it contains several stars (See below Sect. 3.4).

Our imaging of N160A also unveils at least three previously unknown and even smaller ionized regions of size  $\sim 1''$  located in the vicinity of A2. They appear as reddish spots on the true color image, and are centered on stars #108, #29, and #72. The reason for the color is either a cooler temperature of their exciting stars or higher extinction due to the presence of dust.



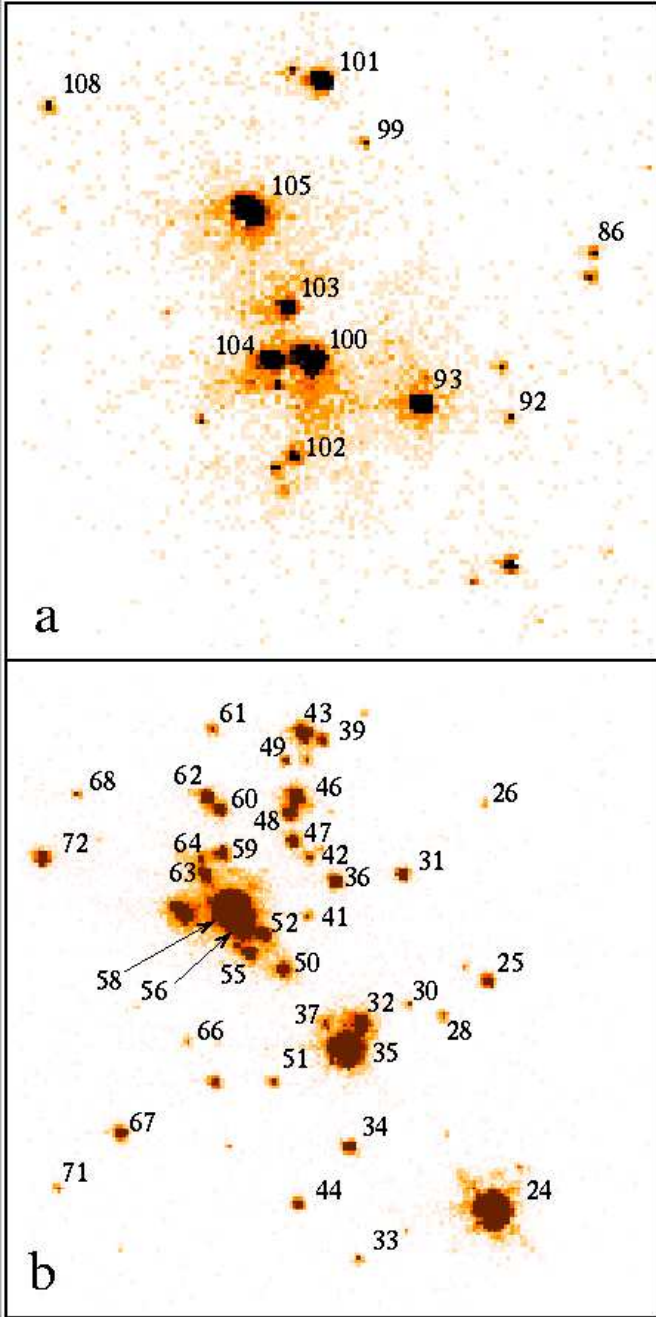


**Fig. 3.** Details of the *HST*/WFPC2 image in the Strömgren  $y$  filter showing: a) the star cluster towards the compact H II region A2. The central components are probably the exciting stars of A2, with star #105 ( $y = 16.82$  mag) being the main one. The field size is  $\sim 8'' \times 8''$  ( $2 \text{ pc} \times 2 \text{ pc}$ ). b) The central star cluster lying between the compact H II regions A1 and A2. The field size is  $\sim 9''.3 \times 8''.5$  ( $2.3 \text{ pc} \times 2.1 \text{ pc}$ ) and the orientation is as in Fig. 2.

### 3.2. Extinction

A map of the  $H\alpha/H\beta$  Balmer decrement is presented in Fig. 4a and it further confirms that the H II region N160A is generally affected by a considerable amount of

interstellar dust. More importantly, it displays for the first time the spatial distribution of the dust over the H II region. It is evident from this map that the dust is not uniformly distributed but is rather “patchy” in nature. In particular a remarkable quantity of dust is concentrated behind the large western ionization front where the  $H\alpha/H\beta$  ratio has an average value of 4.76 ( $A_V = 1.4$  mag) and peaks at as high as 6.33 ( $A_V = 2.2$  mag). The highest dust content though can be found further west of this front, where the Balmer decrement has a mean value of 5.44 ( $A_V = 1.8$  mag) reaching up to 6.87 ( $A_V = 2.5$  mag). The average value of  $H\alpha/H\beta$  towards the central regions of N160A is 4.25 ( $A_V = 1.1$  mag).

As one would expect, the two blobs lie in very dust rich areas of the region. For A1 dust is mainly located behind the southern border of the cavity, where the mean and maximum value of the Balmer decrement is 4.50 ( $A_V = 1.3$  mag), and 5.18 ( $A_V = 1.7$  mag) respectively. Interestingly, the northern compact H II region A2 is more affected by dust, covering a more extended area with a mean Balmer decrement of 4.90 ( $A_V = 1.5$  mag) and attaining a maximum value of 5.50 ( $A_V = 1.8$  mag). The extinction values reported here revise the preliminary estimates given in Paper I.

The  $H\alpha/H\beta$  map was also used to accurately correct the  $H\beta$  flux of the H II region for interstellar reddening. The correction was applied to the  $H\beta$  image on a pixel by pixel basis using straightforward mathematical operations.

### 3.3. Nebular emission

The  $[O III]\lambda 5007/H\beta$  intensity map displaying the excitation of the H II region N160A is presented in Fig. 4b. A remarkable feature is the compact H II region A1 which stands out as the most excited part of N160A. The bubble-shape nature of A1, apparent in Fig. 1, is also obvious in lower contrast images of the  $[O III]/H\beta$  ratio, confirming the presence of a strong wind from the hot exciting star. The mean value of the ratio of the shell surrounding the cavity is  $\sim 6.5$ , with several localized peaks of  $> 7$ . The map also reveals that the curved ridge west of A1 is quite excited with a mean ratio of  $\sim 5.5$ . In contrast, the compact H II region A2 is less excited, the  $[O III]/H\beta$  ratio getting a mean value of  $\sim 4.5$  and never exceeding  $\sim 5$ . Outside the compact regions A1 and A2, the ratio has a mean value of  $\sim 4$ , but it extends over the whole N160A. This means that the  $O^{++}$  ions occupy almost the same volume as  $H^+$  necessitating the presence of several ionizing sources.

The total  $H\beta$  flux of N160A was derived using the method described in Section 3.2. The corrected flux is  $F_0(H\beta) = 2.20 \times 10^{-10} \text{ erg cm}^{-2} \text{ s}^{-1}$  above  $3\sigma$  level accurate to 5%. Assuming that the H II region is

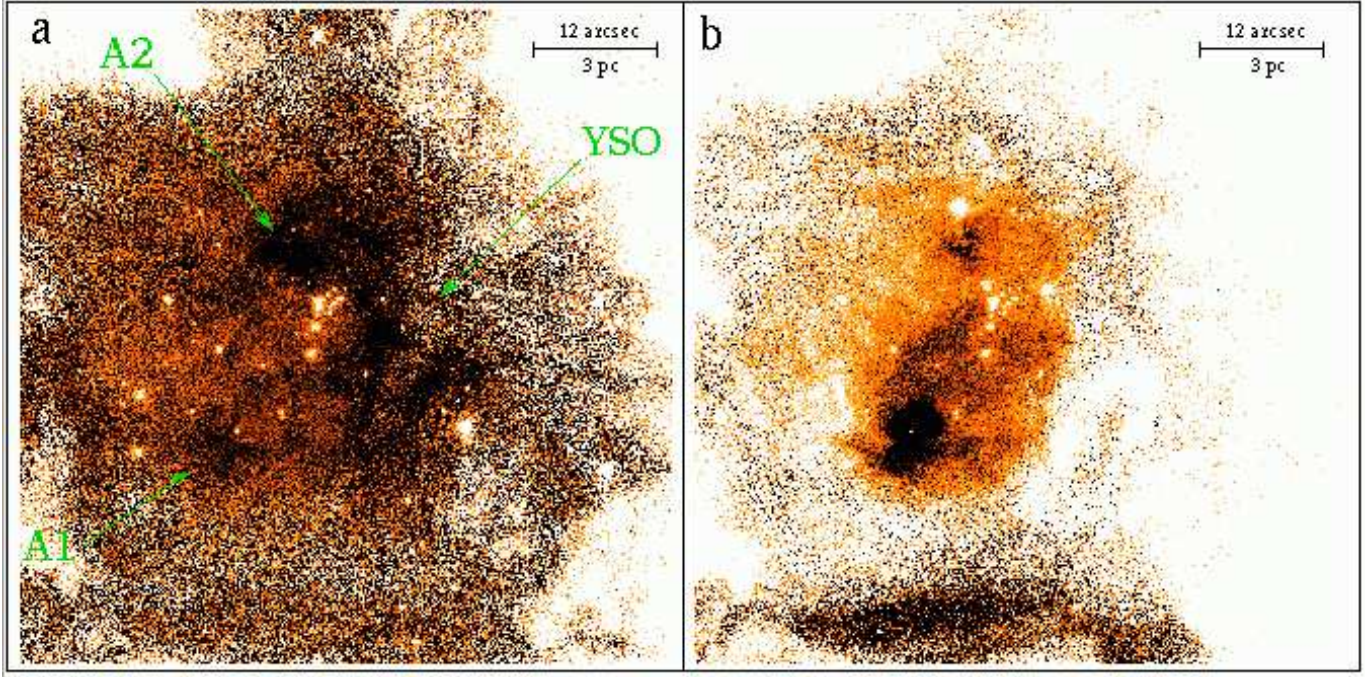


**Fig. 4.** Line intensity ratios for the LMC compact nebula N160A. Darker colors correspond to higher ratio values. The field of view and orientation are identical to Fig. 1. The white spots are stars and can be identified using Figs. 2 and 3. **a)** Balmer decrement  $H\alpha/H\beta$ . Its mean value over the diffuse component is  $\sim 4.25$  ( $A_V = 1.1$  mag), while the ratio goes up to  $\sim 4.5$  ( $A_V = 1.3$  mag) and  $4.9$  ( $A_V = 1.5$  mag) towards the compact blobs A1 and A2 respectively. The position of the infrared young stellar object (see text) is indicated. **b)** The  $[O III]\lambda 5007/H\beta$  ratio. The mean value for the nebula outside the blobs is  $\sim 4$ , reaching its peak ( $> 7$ ) towards A1.

ionization-bounded, the corresponding Lyman continuum flux of N160A is  $N_L = 1.70 \times 10^{50}$  photons  $s^{-1}$ . Several combinations of stars of various types can account for the observed ionizing UV flux: two O3 V and one O6 V star, three O4 V and one O6 V star, or even five O5 V and one late O or one B0 V star (Vacca et al. 1996, Schaerer & de Koter 1997). However these fluxes are probably underestimates since the H II region is more than likely not completely ionization-bounded, due to the fact that it has become open to the interstellar medium in the direction of the observer.

In a similar manner one can estimate the dereddened  $H\beta$  fluxes of both HEBs. We find that  $F_0(H\beta) = 1.10 \times 10^{-11}$  in A1, and  $1.55 \times 10^{-11}$  erg  $cm^{-2}$   $s^{-1}$  in A2, accurate to 20 and 30% respectively. Note that even though the un-corrected images show the contrary, A2 is intrinsically more luminous than A1 because it is more dusty. The corresponding estimated Lyman continuum photon fluxes are  $N_L = 8.50 \times 10^{48}$  photons  $s^{-1}$  for A1 and  $N_L = 1.20 \times 10^{48}$  photons  $s^{-1}$  for A2. A single main sequence star of type earlier than O7.5–O8 can account for the ionizing flux of A1, while in the case of A2 it should be at least an O7–O7.5.

### 3.4. Stellar content

The *HST* images reveal some 110 stars brighter than  $y \sim 21$  mag across N160A. The brightest ones are grouped in a central cluster extending over an area  $\sim 9'' \times 8''$  between the two compact H II regions A1 and A2. The brightest component of the cluster, star #58, has  $y = 14.56$  mag, and it is followed by stars #24, #35, and #56 with  $y = 14.70, 15.08$ , and  $15.23$  mag respectively. The region around star #58 is rather crowded so it is likely that it contains more stars which are not resolved with the PC2.

As we mentioned in Section 3.1, the images of blob A1 uncover only one relatively bright star, #22 with  $y = 15.66$  mag, lying inside it. The star should be a massive O type because it has sculpted a cavity and produced the highest  $[O III]/H\beta$  ratio in the whole region. The second blob A2, contains a dozen rather faint stars, the brightest of which, #105, has a magnitude  $y = 16.82$ . The second brightest star of A2 is #100, with  $y = 17.22$  mag.

Using a cutoff at  $y = 19$  mag, we construct a color-magnitude (C-M) diagram of  $y$  versus  $b - y$  (Fig. 5) for the stars observed across N160A. The diagram displays two principal populations. A main sequence cluster in the interval  $14.56 \leq y \leq 19.00$  is centered around  $b - y \sim -0.05$  mag, while there is a clear spread in colors

due to the important and inhomogeneous dust extinction towards the nebula, discussed in Section 3.2. The second stellar population, of mainly fainter stars, likely consists of very reddened main sequence components and perhaps more evolved field stars. It is quite possible that this latter population is not physically associated with N160A and it may be along a line of sight contamination to this young region.

One could try to estimate the luminosity of the brightest star of the region (#58), although in the absence of spectroscopic data this would not be very accurate. Using a reddening of  $A_V = 1.1$  mag corresponding to the mean value for the associated nebula (Section 3.2), and a distance modulus  $m - M = 18.5$  (e.g. Kovács 2000 and references therein), we find a visual absolute magnitude  $M_V = -5.04$  mag. Following the calibration of Vacca et al. (1996) for Galactic stars, if the star is on the main sequence, it would be an O6.5 V, with a luminosity  $\log L = 5.49 L_\odot$  and a mass  $M = 40 M_\odot$ .

The other massive stars contributing to the ionization of the whole H II region N160A are the brightest members of the central cluster, i.e. #58, #24, #35, and #56. There are also some candidates lying outside the cluster: #84, #107, #75, and #18. We note that star #56 is offset red-wards ( $b - y \sim +0.30$ ) in the C-M diagram. However, its reddened color is due to the presence of dust, since the  $H\alpha/H\beta$  ratio indicates a rather high extinction in that direction, and moreover one of the “small” dust pillars lies there. As a result, star #58 is more than likely intrinsically blue and one of the main exciting stars of the region.

#### 4. Discussion

The resolving power of *HST* makes it possible to see the details of the interplay between the hot gas and prominent dust structures present in this region. In particular, the dust content, which is quite high, increases westward where the remarkable ionization front lies. The front must represent the interface with the molecular cloud component N160-4 which appears to be adjacent to N160A (Johansson et al. 1998). Its physical characteristics given by the latter authors are:  $V_{LSR} = 237.0$  km s<sup>-1</sup>,  $\Delta V = 4.66$  km s<sup>-1</sup>, size 10.3 pc, CO luminosity  $4.2 \times 10^3$  K km s<sup>-1</sup> pc<sup>2</sup>, and virial mass  $3.4 \times 10^4 M_\odot$ .

Furthermore, the  $H\alpha/H\beta$  map, which displays the variation of the dust content across the nebula, shows rather high extinction values. However, since the Balmer decrement is preferentially biased towards emission from the outer regions of the nebula, we cannot probe the deeply embedded IR sources, particularly the young stellar object observed towards N160 (Epchtein et al. 1984, Henning et al. 1998) for which the latter authors find a tremendous extinction of  $A_V = 60 \pm 10$

mag. Nonetheless, using the reported coordinates of  $\alpha(2000) = 5^h 39^m 43^s.8 \pm 0^s.4$ ,  $\delta(2000) = -69^\circ 38' 33'' \pm 2''$  (Henning et al. 1998), we can precisely locate it with respect to the H II region N160A. It lies behind the ionization front in the absorption zone, or put loosely in the “ghost’s mouth” (Figs. 1 and ??)! This situation is very interesting for models studying the sequential star formation (Elmegreen & Lada 1977). According to these models, stars can form from the collapse of a narrow compressed shell between the ionization front and the shock preceding it in the molecular cloud. The YSO may therefore be a newborn star triggered by the ionization front of N160A.

The two HEBs A1 and A2 represent very recent massive star formation events in the N160A region, since all other massive stars have had enough time to disrupt their natal material. Only the YSO can be younger than them. A1, which is of higher excitation than A2, is apparently powered by only one massive star (#22) of type at least O7.5–O8 V. However, other undetected stars may be embedded in the dust and gas. The strong wind of star #22 has carved the cavity or bubble which can be easily seen in the *HST* images, and whose age can be estimated. Assuming a typical mass loss rate of  $6 \times 10^{-5} M_\odot$  yr<sup>-1</sup> for the presumed central O star, a wind velocity of 1000 km s<sup>-1</sup>, a gas density of 1500 cm<sup>-3</sup> (Paper I), and an observed radius of 1''2 (0.3 pc) we find a lifetime of 2500 yr from the classical equations governing the interaction of the stellar wind and the interstellar medium (Weaver et al. 1977, Dyson 1978). Since the estimated density is based on the [S II] doublet, which is sensitive to the outer low density regions, we may underestimate the real density. Should the density be a factor of say 10 larger and the wind velocity a factor of 2 lower, the corresponding age will be 8600 yr, that is very young in any case. As to A2, it may even be younger than A1 due to its heavy dust content. We cannot confirm that all of the detected stars in A2 are massive ones, but the high [O III]/ $H\beta$  ratio and the measured  $H\beta$  flux indicate beyond doubt that massive stars are present.

Several of the N160A candidate stars (#58, #24, #35, and #56) belong to the central cluster, while the rest (#84, #107, #75, and #18) lie far from it. It is quite possible though that these latter stars have been originally members of the central cluster. Models studying formation of massive stars predict that they should never form in isolation (Bonnell et al. 1998), and that those found in isolation have been ejected from dense stellar clusters (Leonard & Duncan 1990, Kroupa 1995). This scenario is particularly attractive for very young massive star regions like N160A where a dense central blue star cluster is present. Escape velocities of newly formed stars can exceed 200 km s<sup>-1</sup> (Leonard & Duncan 1990, Kroupa 1995), but the largest fraction of them (23%) is expected to have values of about 50 km s<sup>-1</sup>. Assuming such a velocity for star #87, which has a projected



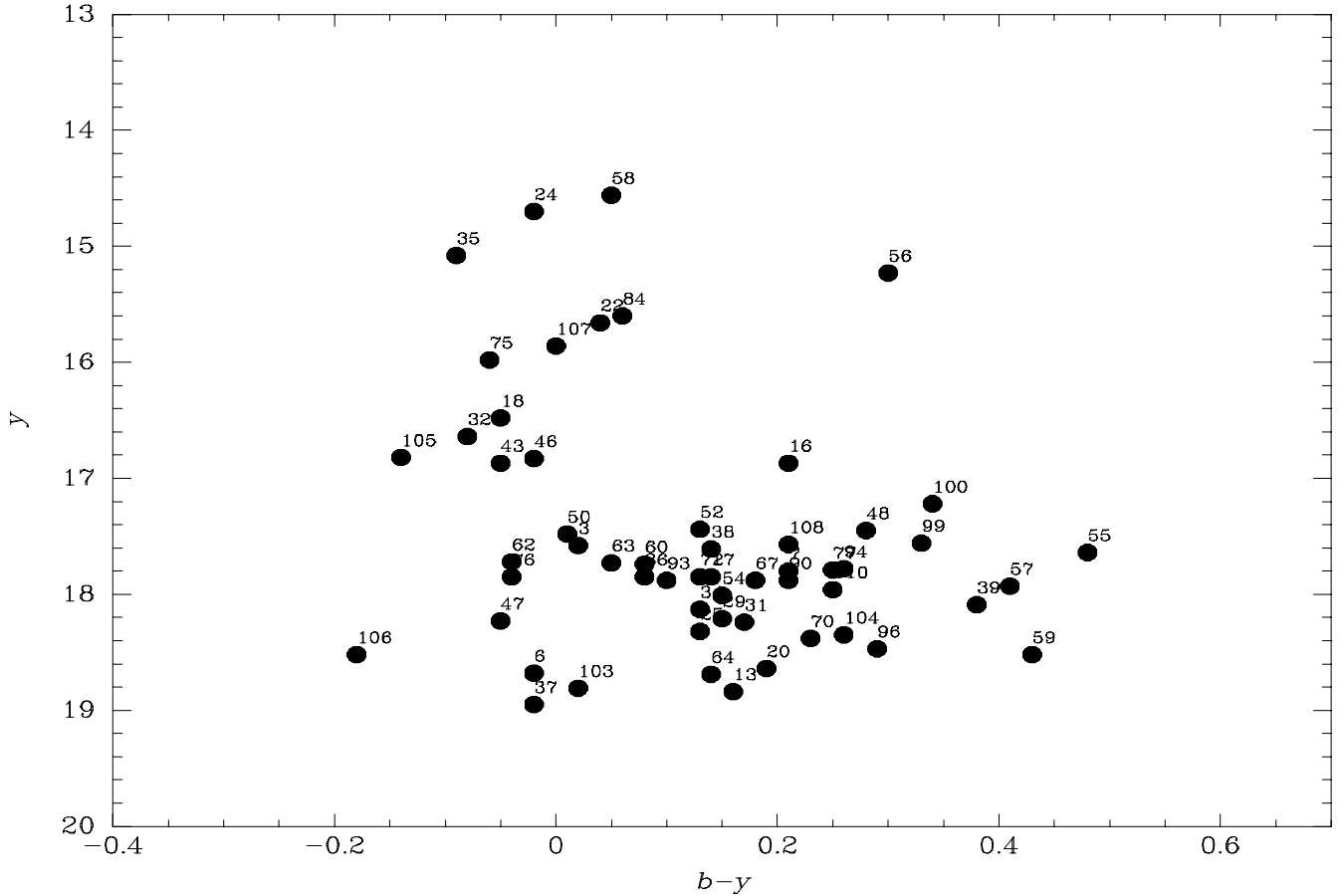


**Fig. 5.** Color-magnitude diagram of the brightest stars (lower cutoff at  $y = 19$  mag) observed towards the H II region N160A based on WFPC2 imaging with the Strömgren filters  $b$  (F467M) and  $y$  (F547M). The magnitudes are not corrected for reddening.

distance of  $\sim 20''$  (5 pc) from the cluster center, it would take some 100 000 years for this star to reach its present position. This estimate is of course a lower limit, since we use projected and not the real distances. Inversely, one can calculate the minimum velocities at which the stars could have reached their current locations. Assuming a lifetime of 3 Myr, one gets a lower ejection velocity of  $\sim 2 \text{ km s}^{-1}$  for #87. One might wonder whether the observed star density of the central cluster is sufficiently high for the dynamical ejection mechanism to work. However, Leonard & Duncan (1988) have shown that binary-binary collisions required to produce high velocity escapees occur in low density clusters, even though simple estimates suggest that such interactions are unlikely. Furthermore, the ejection of the stars must have happened during an earlier evolutionary stage when the cluster was most probably more compact than today (Portegies Zwart et al. 1999).

The population of red stars present in the color-magnitude diagram is expected to actually be on the main sequence but affected by the dust in this young

region. However, with the present data we cannot exclude the presence of evolved and/or lower mass pre-main sequence stars. If evolved stars are really there, this would imply that star formation has occurred in successive waves in this part of the LMC. Whether or not lower mass stars are indeed present in this region is very interesting as it could be a test for the so-called bi-modal star formation concept predicting that high mass stars form without their low mass counterparts (Güsten & Mezger 1982, Zinnecker et al. 1993). The fact that HEBs in general, and N160A in particular, are extremely young provides an unparalleled opportunity for verifying these models.

*Acknowledgements.* We would like to thank the referee Dr. Joel Wm. Parker for his helpful comments which improved the manuscript. VC would like to acknowledge the financial support for this work provided by NASA through grant number GO-8247 from the STScI, which is operated by the Association of Universities for Research in Astronomy, Inc., under NASA contract NAS 5-26555.



## References

- Bonnell I.A., Bate M.R., Zinnecker H., 1998, MNRAS 298, 93
- Brooks K.J., Whiteoak J.B., 1997, MNRAS 291, 395
- Caswell J.L., Haynes R.F., 1981, MNRAS 194, 33P
- Caswell J.L., 1995, MNRAS 272, L31
- Davies, R.D. Elliott K.H., Meaburn J., 1976, MNRAS 81, 89
- Dyson J.E., 1978, A&A 62, 269
- Elmegreen B.G., Lada C.J., 1977, ApJ 214, 725
- Epchtein N., Braz M.A., Sèvre F., 1984, A&A 140, 67
- Gardener F.F., Whiteoak J.B., 1985, MNRAS 215, 103
- Güsten R., Mezger P.G., 1982, Vistas in Astronomy 26, 159
- Henize K.G., 1956, ApJS 2, 315
- Henning Th., Klein R., Chan S.J., Fitzpatrick E.L., et al. 1998, A&A 338, L51
- Heydari-Malayeri M., Testor G., 1986, A&A 162, 180 (Paper I)
- Heydari-Malayeri M., Charmandaris V., Deharveng L., Rosa M.R., Schaerer D., Zinnecker H., 2001, A&A 372, 495
- Holtzman J., Hester J.J., Casertano S., et al., 1995, PASP 107, 156
- Johansson L.B.E., Greve A., Booth R.S. et al., 1998, A&A 331, 857
- Jones T.J., Hyland A.R., Straw S., et al., 1986, MNRAS 219, 603
- Kovács G., 2000, A&A 363, L1
- Kroupa P., 1995, MNRAS 277, 1522
- Leonard, P.J.T., Duncan M.J., 1988, AJ 96, 222
- Leonard, P. J. T., Duncan M.J., 1990, AJ 99, 608
- Lucke P.B., 1974, ApJS 28, 73
- Lucke B.P., Hodge P.W., 1970, AJ 75, 171
- McGee R.X., Milton J.A., 1966, Aust. J. Phys. 19, 343
- Portegies Zwart S.E., Makino J., McMillan S.L.W., Hut P., 1999, A&A 348, 117
- Relyea L.J., Kurucz R.L., 1978, ApJS 37, 45
- Schaerer D., de Koter A., 1997, A&A 322, 598
- Vacca W.D., Garmany C.D., Shull J.M., 1996, ApJ 460, 914
- Weaver R., McCray R., Castor J., et al., 1977, ApJ 218, 377
- Whiteoak J.B., Wellington K.J., Jauncey D.L., et al., 1983, MNRAS 205, 275
- Whiteoak J.B., Gardener F.F., 1986, MNRAS 222, 513
- Zinnecker H., McCaughrean M.J., Wilking B., 1993, in “Protostars and Planets III”, eds. E.H. Levy & J.I. Lunine, Univ. of Arizona Press, Tuscon, p. 429

**Table 2.** *HST* Photometry of the brightest stars towards N160A

Star	RA(J2000)	Dec(J2000)	F300W Wide <i>U</i>	F410M Strömgren <i>v</i>	F467M Strömgren <i>b</i>	F547M Strömgren <i>y</i>	Color <i>b</i> − <i>y</i>
1	5:39:41.1	-69:38:35.0	—	—	—	—	—
2	5:39:41.0	-69:38:49.0	18.60	—	—	—	—
3	5:39:41.0	-69:38:49.2	16.43	17.61	17.60	17.58	0.02
4	5:39:41.3	-69:38:36.9	18.28	19.27	19.22	19.02	0.20
5	5:39:41.5	-69:38:31.8	18.53	19.94	19.30	—	—
6	5:39:41.4	-69:38:33.7	17.32	18.77	18.66	18.68	-0.02
7	5:39:41.6	-69:38:30.3	16.44	17.96	18.01	17.80	0.21
8	5:39:41.5	-69:38:38.9	—	—	—	—	—
9	5:39:41.7	-69:38:33.8	18.69	—	—	—	—
10	5:39:42.0	-69:38:32.6	18.39	—	—	—	—
11	5:39:42.1	-69:38:37.3	—	—	—	—	—
12	5:39:42.6	-69:38:41.0	17.67	19.53	19.35	18.94	0.41
13	5:39:42.3	-69:38:56.7	17.40	18.92	19.01	18.84	0.17
14	5:39:42.5	-69:38:54.2	18.18	19.88	19.50	19.55	-0.05
15	5:39:42.8	-69:38:42.9	18.12	19.83	19.79	19.58	0.21
16	5:39:43.0	-69:38:38.6	15.89	17.04	17.08	16.87	0.21
17	5:39:43.1	-69:38:48.7	16.98	18.10	17.99	17.85	0.14
18	5:39:43.2	-69:38:48.5	15.23	16.45	16.43	16.48	-0.05
19	5:39:43.4	-69:38:44.9	—	—	—	—	—
20	5:39:43.4	-69:38:41.6	17.38	18.79	18.83	18.64	0.19
21	5:39:43.2	-69:38:58.2	18.56	—	—	—	0.97
22	5:39:43.4	-69:38:53.6	14.27	15.55	15.70	15.66	0.04
23	5:39:44.0	-69:38:32.8	18.24	19.57	19.38	19.04	0.34
24	5:39:43.9	-69:38:42.4	13.22	14.51	14.68	14.70	-0.02
25	5:39:44.0	-69:38:39.4	17.25	18.29	18.45	18.32	0.13
26	5:39:44.0	-69:38:37.1	18.55	—	—	—	—
27	5:39:44.1	-69:38:35.8	—	—	—	—	—
28	5:39:44.1	-69:38:40.0	18.68	19.46	19.80	19.49	0.31
29	5:39:44.3	-69:38:32.9	16.97	18.32	18.36	18.21	0.15
30	5:39:44.2	-69:38:39.9	—	—	—	—	—
31	5:39:44.2	-69:38:38.2	16.93	18.28	18.41	18.24	0.17
32	5:39:44.3	-69:38:40.2	15.28	16.46	16.56	16.64	-0.08
33	5:39:44.2	-69:38:43.2	19.58	—	—	19.71	—
34	5:39:44.3	-69:38:41.8	16.95	18.15	18.26	18.13	0.13
35	5:39:44.3	-69:38:40.5	13.67	14.88	14.99	15.08	-0.09
36	5:39:44.4	-69:38:38.3	16.59	17.73	17.93	17.85	0.08
37	5:39:44.4	-69:38:40.2	18.10	18.98	18.93	18.95	-0.02
38	5:39:44.3	-69:38:47.4	15.90	17.58	17.75	17.61	0.14
39	5:39:44.5	-69:38:36.5	17.50	18.65	18.47	18.09	0.38
40	5:39:44.5	-69:38:32.7	18.77	—	—	—	—
41	5:39:44.5	-69:38:38.8	—	19.84	19.88	—	—
42	5:39:44.5	-69:38:38.1	18.73	19.77	19.16	19.27	-0.11
43	5:39:44.5	-69:38:36.5	15.71	16.94	16.82	16.87	-0.05
44	5:39:44.4	-69:38:42.6	18.03	18.62	18.93	18.66	0.27
45	5:39:44.2	-69:38:53.6	18.23	—	—	19.58	—
46	5:39:44.5	-69:38:37.3	15.68	16.84	16.81	16.83	-0.02
47	5:39:44.5	-69:38:37.9	16.99	18.28	18.18	18.23	-0.05
48	5:39:44.5	-69:38:37.5	16.65	17.67	17.73	17.45	0.28
49	5:39:44.6	-69:38:36.9	19.65	—	19.52	19.85	-0.33
50	5:39:44.5	-69:38:39.6	16.29	17.45	17.49	17.48	0.01
51	5:39:44.5	-69:38:41.0	18.52	19.56	19.74	19.51	0.23
52	5:39:44.6	-69:38:39.2	16.41	17.70	17.57	17.44	0.13
53	5:39:44.6	-69:38:35.6	18.51	—	—	—	—
54	5:39:44.3	-69:38:56.4	16.54	17.94	18.16	18.01	0.15
55	5:39:44.6	-69:38:39.4	16.90	17.97	18.12	17.64	0.48
56	5:39:44.6	-69:38:39.0	14.05	15.56	15.53	15.23	0.30
57	5:39:44.6	-69:38:39.3	17.48	18.11	18.34	17.93	0.41
58	5:39:44.7	-69:38:38.8	13.26	14.48	14.61	14.56	0.05
59	5:39:44.7	-69:38:38.2	18.14	18.89	18.95	18.52	0.43
60	5:39:44.7	-69:38:37.6	16.61	17.87	17.82	17.74	0.08

Star	RA(J2000)	Dec(J2000)	F300W Wide <i>U</i>	F410M Strömgren <i>v</i>	F467M Strömgren <i>b</i>	F547M Strömgren <i>y</i>	Color <i>b - y</i>
61	5:39:44.8	-69:38:36.5	17.84	19.19	19.36	19.03	0.33
62	5:39:44.8	-69:38:37.4	16.51	17.57	17.68	17.72	-0.04
63	5:39:44.7	-69:38:38.4	16.79	17.78	17.78	17.73	0.05
64	5:39:44.7	-69:38:38.2	18.95	18.56	18.83	18.69	0.14
65	5:39:44.6	-69:38:48.1	18.69	—	—	—	—
66	5:39:44.7	-69:38:40.6	—	—	—	19.81	—
67	5:39:44.9	-69:38:41.9	16.70	17.89	18.06	17.88	0.18
68	5:39:45.1	-69:38:37.6	18.55	19.90	19.84	19.71	0.13
69	5:39:45.2	-69:38:34.0	18.48	—	—	19.84	—
70	5:39:45.2	-69:38:33.6	17.08	18.41	18.61	18.38	0.23
71	5:39:45.0	-69:38:42.7	19.43	—	—	19.83	—
72	5:39:45.2	-69:38:38.4	16.90	17.98	17.98	17.85	0.13
73	5:39:45.0	-69:38:47.2	18.27	—	—	19.28	—
74	5:39:45.4	-69:38:31.6	19.00	19.36	19.27	18.81	0.46
75	5:39:45.0	-69:38:50.4	14.51	15.92	15.92	15.98	-0.06
76	5:39:45.2	-69:38:40.5	16.64	17.85	17.81	17.85	-0.04
77	5:39:45.4	-69:38:33.6	16.44	17.85	18.04	17.79	0.25
78	5:39:45.4	-69:38:32.2	18.77	—	—	19.59	—
79	5:39:45.3	-69:38:38.7	18.98	—	—	19.98	—
80	5:39:45.2	-69:38:47.4	18.80	—	—	—	—
81	5:39:45.0	-69:38:58.0	17.88	19.30	19.36	19.00	0.36
82	5:39:45.4	-69:38:41.4	18.79	19.98	—	19.86	—
83	5:39:45.4	-69:38:46.7	17.96	19.95	19.67	19.52	0.15
84	5:39:45.1	-69:39:00.1	14.06	15.47	15.66	15.60	0.06
85	5:39:45.2	-69:38:55.6	18.12	19.89	—	19.51	—
86	5:39:45.6	-69:38:36.8	19.62	—	—	—	1.15
87	5:39:45.2	-69:39:00.3	18.98	19.62	19.58	19.48	0.10
88	5:39:45.5	-69:38:52.2	17.92	19.56	19.61	19.14	0.47
89	5:39:45.4	-69:38:56.1	17.57	19.18	19.15	18.98	0.17
90	5:39:45.7	-69:38:41.6	16.77	17.91	18.09	17.88	0.21
91	5:39:45.3	-69:39:02.2	18.47	19.57	—	19.36	—
92	5:39:45.8	-69:38:38.4	19.49	—	—	—	—
93	5:39:45.9	-69:38:38.4	16.71	17.87	17.98	17.88	0.10
94	5:39:45.5	-69:39:01.0	16.52	17.92	18.04	17.78	0.26
95	5:39:45.8	-69:38:43.4	19.95	—	—	—	—
96	5:39:45.7	-69:38:51.2	17.32	18.59	18.76	18.47	0.29
97	5:39:45.9	-69:38:43.4	19.00	—	—	—	—
98	5:39:45.7	-69:38:52.2	18.18	—	—	19.88	—
99	5:39:46.1	-69:38:35.5	16.43	17.68	17.89	17.56	0.33
100	5:39:46.1	-69:38:38.0	16.30	17.62	17.56	17.22	0.34
101	5:39:46.2	-69:38:34.8	18.59	19.39	19.72	19.27	0.45
102	5:39:46.1	-69:38:38.9	18.52	19.67	19.65	19.82	-0.17
103	5:39:46.2	-69:38:37.6	19.53	19.30	18.83	18.81	0.02
104	5:39:46.2	-69:38:38.1	17.21	18.48	18.61	18.35	0.26
105	5:39:46.2	-69:38:36.7	15.37	16.76	16.68	16.82	-0.14
106	5:39:45.9	-69:39:02.8	17.13	18.45	18.34	18.52	-0.18
107	5:39:46.4	-69:38:52.1	14.41	15.75	15.86	15.86	0.00
108	5:39:46.7	-69:38:36.4	16.29	17.54	17.78	17.57	0.21
109	5:39:46.7	-69:38:48.9	18.19	—	19.03	19.17	-0.14
110	5:39:46.8	-69:38:44.4	16.60	18.10	18.21	17.96	0.25